



ORIGINAL RESEARCH PAPER

Study on the effectiveness of commercial anti-islanding algorithms in the prospect of mass penetration of PVs in low-voltage distribution networks

Alexandros Boubaris¹ | Anastasios Kyritsis² | Konstantinos Babouras¹ |
Syllas Frantzeskakis¹ | Nick Papanikolaou¹ | Theofilos Papadopoulos¹ |
Iñigo Vidaurrezaga³ | Ricardo Alonso³

¹ECE Department, Democritus University of Thrace, Xanthi, Greece

²Department of Environment, Ionian University, Zakynthos, Greece

³Tecnalia Research & Innovation, Parque Científico y Tecnológico de Bizkaia, Derio, Spain

Correspondence

Nick Papanikolaou, ECE Department, Democritus University of Thrace, V. Sofias 12, Xanthi, Greece.
Email: npapanik@ee.duth.gr

Funding information

Horizon 2020 (EriGrid), Grant/Award Number: 654113

Abstract

In the coming years, distribution grids will be progressively flooded by renewable energy sources (RES) that will be interconnected with the main grid through power electronic converters. Photovoltaics (PVs) are one of the most promising renewable technologies even for densely built-up areas where space problems are inevitable. The high penetration prospect of PV facilities on low-voltage distribution networks raises questions regarding the necessity of advanced functions that will enable electronically coupled RES to support the operation of distribution grids and to enhance their reliability. In this context, the objective of this study is to investigate the effectiveness of various islanding prevention measures installed in commercial PV inverters, when multiple inverters are operating in parallel with a low-voltage distribution network (LVDN). Extensive experiments were performed under various PV penetration levels, linear/non-linear load and over/under voltage and over/under frequency conditions, as well as for various values of total harmonic distortion of the mains voltage. Further to the primary statistical analysis, the results were analysed in depth by advanced mathematical methods such as box plot and cluster analysis. The findings of this study indicate that commercial anti-islanding techniques present a high probability of failure in the case of multiple PV units at the same point of common coupling, calling for new and more advanced algorithms.

1 | INTRODUCTION

The need to mitigate the dependence on fossil fuels has led to new mandates to replace fossil-based electricity generation with renewable energy sources (RES). Solar photovoltaics (PVs) are among those resources, being an environmentally friendly and sustainable investment [1,2].

Indeed, during the last decade, PVs have been the fastest growing RES worldwide. The use of different topologies of power electronic converters enables the exploitation of solar PV energy both in large power plants and in small-scale residential installations connected to low-voltage distribution networks (LVDNs) [3]. Considering that high numbers of such photovoltaic applications are expected in the near future, structural changes in distribution networks are expected, giving

rise to concerns about their reliable and secure operation [4]. Additionally, in future electrical systems and networks (such as smart grids, micro grids, web of cells etc.) a vast amount of conventional rotating generators will be replaced by electronically coupled RES (mainly PVs at the distribution level). Therefore, a high PV penetration level (PL) may jeopardise the stability of the power system due to their variability and intermittency [5].

One of the main concerns that emerges when multiple PV inverters are connected to the same point of common coupling (PCC) in the LVDN is the detection of unintentional islanding operation. The main reason for this concern is that anti-islanding algorithms of current commercial inverters are not properly designed to counter this forthcoming grid condition [6–9].

This is an open access article under the terms of the Creative Commons Attribution License, which permits use, distribution and reproduction in any medium, provided the original work is properly cited.

© 2021 The Authors. *IET Energy Systems Integration* published by John Wiley & Sons Ltd on behalf of The Institution of Engineering and Technology and Tianjin University.

The above concerns are supported by several scientific works, which highlight that the effectiveness of well-known and widespread anti-islanding techniques (such as the impedance measurement monitoring techniques, the active frequency drift monitoring technique, the frequency bias or frequency shift up/down techniques, the frequency jump technique, the Sandia frequency shift monitoring technique, the accelerated frequency drift, the active frequency drift with positive feedback and the “follow the herd” technique) decreases in the case of parallel, uncoordinated operation of multiple inverters [10–13]. However, techniques such as the impedance detection at a specific frequency monitoring (usually a sub-harmonic one) or the slip-mode frequency shift monitoring are not affected in the case of parallel operation of multiple inverters; on the one hand, the presence of sub-harmonics due to those techniques may cause saturation issues to the distribution transformers (depending on the sub-harmonic component amplitude), whereas power quality degradation and transient phenomena are inevitable in the case of high PL of PVs [14]. Additionally, the parallel operation of PV inverters employing sophisticated anti-islanding techniques (where single or dual harmonic injection techniques are adopted [15,16]), may cause deformation of the detection zone [17] affecting the detection time frame [18], whilst in some case it may cease the operation of PV inverters even under normal operation.

Additionally, new advanced distributed energy resources (DER) functions such as the dynamic reactive current support mode and low-voltage-ride-through requirements (LVRT), that were discussed under California Rule 21 [19] and adopted by IEEE 1547-2018, may have a negative impact on the effectiveness of current commercial islanding detection schemes [20]. Therefore, it is expected to increase the number of undetected island events, thereby increasing the shock hazard of unsuspecting utility line workers (who think that the lines are not energised), as well as endangering the safety of consumers and utility equipment that are interconnected with LVDN [21,22].

To conclude, based on the existing scientific literature, it is presumed that the emerging topic of multiple PV inverters (employing various anti-islanding protection algorithms) at the same PCC has not been sufficiently investigated yet [23,24]. At this point, it is imperative to highlight that some sophisticated anti-islanding schemes that use advanced techniques for the mitigation of current harmonics components, such as [25–28], are excluded from this study, due to the fact that they have not been widely employed by commercial PV inverters yet. It is recalled that this study focuses on the cooperative response of the commercial PV inverters, which are widely used and established in markets. In this context, the main scope here is to perform a thorough experimental study on the parallel operation of multiple commercial PV inverters at the same PCC and investigate the interactions between them under various PLs [29,30]. For this purpose, a test bench composed of different types of commercial PV inverters (e.g. single-phase [1ph] string inverters, three-phase [3ph] multi-string inverters and module-integrated inverters [MICs]) was employed. The experimental evaluation was conducted at TECNALIA Smart

Grids Testing & Research premises ‘InGRID’, within the framework of the EriGrid/Multi-Island Project [31].

This proposed experimental evaluation (discussed in the next section) is essential in order to understand the changes in output characteristics of PV inverters during the transition from grid-connected to islanded operation and to capture the disconnection time (DT) at which inverters detect the island condition and cease to energise the utility line. At this point, it is noted that DT is mainly affected by the anti-islanding method that each PV inverter adopts, as well as by grid and load conditions [32]. In general, PV inverters do not facilitate an inertia option in their outputs, and thus they can respond immediately to any utility disturbance (such as a frequency shift) [33]. Additionally, most PV inverters sense a short circuit by an associated voltage drop, rather than by sensing a short circuit current [34]. PV PLs also affect DT, because their cumulative energy production may suffice the load demand. It is noted that regardless PV PLs and the number and types of parallel interconnected inverters, PV inverters should disconnect without creating self-sustained islands [35].

A vast amount of experimental data were collected from the above-mentioned test bench for various PLs of PVs, loads and grid conditions (that are described in detail below). Thereafter, these data have been processed accordingly, in order to analyse their effect on successful anti-islanding detection.

Considering the multi-variable character of this study, it is presumed that a general descriptive statistical analysis would be insufficient for the examination of the impact of each factor. It has therefore been necessary to use advanced statistical analysis tools in order to delve into the factual issues that mainly affect inverters behaviour. Techniques such as cluster analysis are proposed for similar power systems studies [36,37] in order to group data into homogeneous classes with similar features. Additionally, cluster analysis is frequently used in distribution systems studies [38], where multiple parameters are changing continuously. One of the most robust algorithms for this demanding activity is the k-means++ algorithm, due to its potential to produce tighter clusters compared to hierarchical clustering [39]. For these reasons, the k-means++ algorithm cluster analysis was employed in order to conclude with an insightful statistical analysis of the experimental results.

In Section 2 the experimental setup is described, whereas the experimental procedure and the parameters of this study are analysed in Section 3. Section 4 summarises the experimental results, whilst in Section 5 the statistical analysis of the key findings takes place. Finally, Section 6 concludes the main outcomes.

2 | SYSTEM DESCRIPTION

The generic scheme of the test bench is illustrated in Figure 1 [40,41]. It consists of the commercial inverters listed in Table 1 (connected to the same PCC), the local load, the PV simulators and grid emulator (Pacific Power Source), and the data

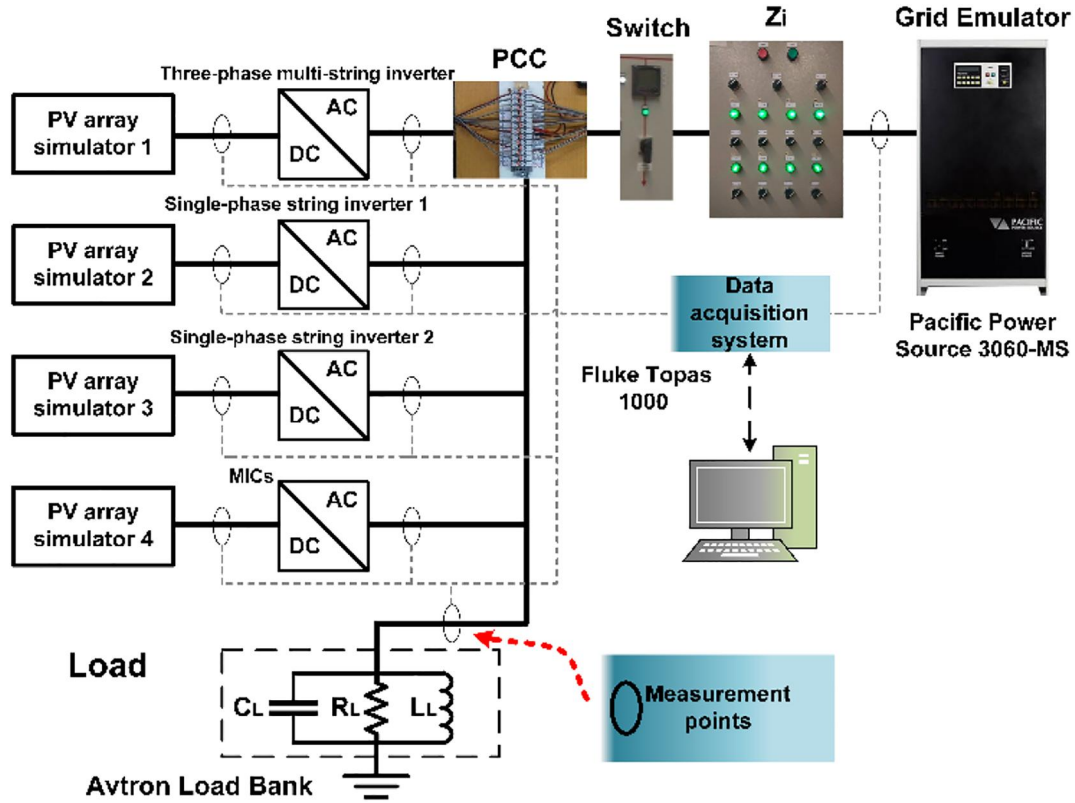


FIGURE 1 Setup of the experimental test bench

TABLE 1 Commercial inverters of the experimental procedure

| Inverter number | Nominal power (W) | Inverter type | Anti-Islanding Method |
|-----------------|-------------------|------------------|--------------------------|
| Inv. 1 | 4500 | 3ph multi-string | Reactive power injection |
| Inv. 2 | 1000 | 1ph string | Impedance measurement |
| Inv. 3 | 1000 | 1ph string | Impedance measurement |
| Inv. 4 | 2×300 | 1ph MIC | Active power deviation |

acquisition system (Fluke Topas 1000 power quality analyser and a multichannel Yokogawa SL1000 oscilloscope).

The waveform capturing/recording device has been selected to capture the output electrical characteristics of each inverter from the beginning of the islanding test until the under-test inverters cease to energise the island, with a resolution better than 1 ms. Additionally, the measurement equipment recorded each phase current and each phase-to-neutral voltage in order to determine real and reactive power flow during every test. The sampling rate was higher than 10 kHz, whilst the minimum measurement accuracy was less than 1% of rated output voltage and current values of each inverter. It is noted that the grid emulator simulates the low-voltage distribution grid, that is 0.4 kV.

The test bench, for evaluating the islanding detection functions of the commercial inverters under-study, was based on the recommended circuit of IEEE 929-2000, IEEE 1547.1 and IEC 62,116 [42,43], where the switch in Figure 1 determines the island condition, as the relevant standard indicates. Additionally, the Z_i -box allows the appropriate

selection of resistance and inductance values and thus we can simulate the internal impedance of the distribution network at the PCC; in LVDN the resistive component is usually the dominant one, so it cannot be omitted from the test bench [44].

As a final point, the methodology of the test parametrisation is described in more detail based on the international standards indications; that is, after the selection of the desirable PL, the proper combination of inverters is set. Subsequently, according to the paragraph 6 of the IEC 62116 standard, the input voltage level of the inverters is specified along with their output power (with proper regulation of the PV array simulator of Figure 1). The scheduling of the mentioned PV simulators follows the directions of 5.2 paragraph of the IEC 62116. Finally, the total grid quality degradation is selected by means of single harmonic amplitude, THD frequency and voltage level, negative sequence, and so on, where the grid emulator of Figure 1 is regulated based on the rules of IEC 62116 standard as described in its 5.3 paragraph.

3 | EXPERIMENTAL PROCEDURE

In terms of power quality, grid-tied inverters should not exceed the limits of the relevant power quality standards [45,46] regarding the maximum permitted magnitude of injected harmonic current components. In addition, the total harmonic distortion (THD) of the inverter output current should be strictly limited to 5%. Additionally, according to the relevant international standard for the evaluation of islanding prevention measures [47], the utility grid (the grid emulator for our case) should meet the following conditions: voltage THD <2.5%, voltage and frequency values should not vary more than $\pm 2.5\%$ and ± 0.1 Hz, respectively, whilst in the case of three-phase operation the phase difference should be in the range of $120^\circ \pm 1.5^\circ$. In the prospect of mass PL of electronically coupled RES, the experimental pattern was tested not only in line with the relevant standard, but also for broadened grid distortion levels as outlined hereafter.

3.1 | General description

Various combinations of parallel-connected inverters, as well as each inverter solely, were tested in order to capture the amount of time that an unintentional island condition exists before the commercial islanding prevention measures cease the inverter operation. For each combination, various grid conditions were applied, as depicted in Figure 2. It should be noted that the term ‘grid conditions’ refers to the selected values of the experimental parameters, that is the grid impedance characteristics, the voltage distortion at PCC, and the under/over

voltage/frequency (UOVF) conditions; in addition, load type (linear or not) was also a parameter of this study. Details on every parameter are given below.

In every test, PV power production meets load power consumption, but not necessarily the nominal power level of the inverters. It is recalled that the load matching condition constitutes the worst-case scenario as it increases the possibility of creating self-sustaining islands.

With the prospect of high PL of PVs in the distributed networks, the grid impedance characteristics became test parameters in order to emulate strong and weak grid conditions [48]. In more detail, the lower the impedance of a distribution network (Z_g) the stronger is the network. Z_g values were introduced into the experimental setup by selecting the appropriate values of R_g and X_g (Z_i box). R_g and X_g represent the equivalent internal resistance and reactance respectively (at the mains angular frequency). It is noted that, according to [49], low values of X_g/R_g ratio (e.g. below 0.5) indicate weak grids, whilst strong grids are characterised by values higher than unity [50]. The selected grid impedance characteristics are listed in Table 2.

TABLE 2 Grid impedance cases

| | R_g (Ohm) | X_g (Ohm) | Z_g (Ohm) |
|-------|-------------|-------------|-------------|
| Z_1 | 3.11 | 1.13 | 3.31 |
| Z_2 | 2.2 | 1.13 | 2.48 |
| Z_3 | 0.36 | 0.98 | 1.04 |
| Z_4 | 0.05 | 0.15 | 0.15 |

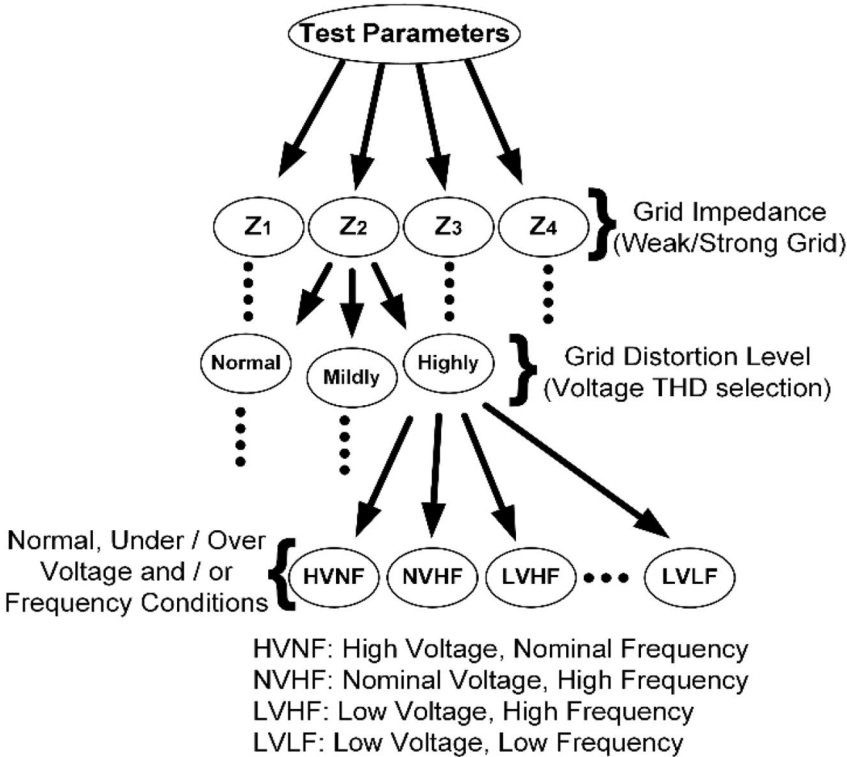


FIGURE 2 Tree diagram of the investigated grid conditions

From another point of view, the characterisation of a network as strong or weak can be based on the value of the P_{PV}/S_{SC} ratio [11], which is calculated according to Equation (1).

$$\frac{P_{PV}}{S_{SC}} = \frac{(R_g^2 + X_g^2)^{1/2}}{R_L} \quad (1)$$

P_{PV} is the nominal power of the installed PV system at PCC, S_{SC} is the short-circuit power at PCC, and R_L is the equivalent load resistance of the islanded network. In accordance with this criterion, P_{PV}/S_{SC} values lower than 0.2 correspond to weak grid conditions. This criterion is particularly useful for the experimental study of the islanding phenomenon. In more detail, by selecting the power production level of the parallel-connected PV inverters (P_{PV}) and their PL (appropriate selection of P_{PV}/S_{SC} ratio), the values of R_g and X_g can be easily selected. Finally, the value of R_L is selected upon the produced PV power level and the desired value of the load quality factor.

3.1.1 | Grid distortion

As regards voltage quality at PCC, it was considered appropriate to study some representative mildly and highly distorted scenarios, where in highly distorted ones a high second-order harmonic component was incorporated. This was considered necessary, in order to take into account some new islanding detection techniques that inject low-order harmonics (impedance monitoring at a specific frequency e.g. second or fourth) as well as their effect on the operation of current commercial inverters [51,52]. Nevertheless, voltage distortion was always kept within the limits set by EN 50160 standard [53], that is THD < 8%, and second, third, fifth, seventh and 11th order harmonics below 2%, 5%, 6%, 5% and 3.5%, respectively. The selected scenarios and the corresponding voltage harmonic distortion profiles are listed in Table 3. As far as weak grid conditions are concerned, two different scenarios were examined both for the mildly (mildly-1 and mildly-2) and the highly (highly-1 and highly-2) distorted LV grids. This was deemed necessary because some of the commercial inverters failed to connect to the PCC under the initial mildly-1 and highly-1 voltage distortion scenarios. Thus, it was imperative to reschedule the initial plan, forming the mildly-2 and highly-2

scenarios strictly below mildly-1. It is worth noting that nowadays all commercial PV inverters that comply with IEEE Std 1547 have been tested for grids with a voltage THD value less than 2.5% and single voltage harmonics amplitudes less than 50% of the absolute limits mentioned in this standard. However, as long as the PL of PVs is increasing, voltage harmonic distortion will play a key role in grid performance and voltage stability. Therefore, the analysis of inverter behaviour under various harmonic distortion conditions is of crucial importance for the reliable and secure operation of future grids.

3.1.2 | UOVF conditions

Voltage-frequency conditions are also important parameters for the performance of anti-islanding techniques. The following conditions were considered: under/over voltage (+10%, -15% voltage deviation) and under/over frequency conditions (symmetrical, ± 0.5 Hz frequency deviation). Additionally, voltage unbalanced conditions were also considered, with the negative sequence component of the supply voltage to be set to 2% of the positive sequence component. This test is meaningful only when the 3ph-inverter is included in the experimental setup. It is noted that the term 'Normal Condition' refers to the balanced 400 Vrms/50 Hz voltage supply.

3.1.3 | Linear and non-linear load conditions

Load type was also a parameter during tests. Initially, a linear load was assumed; the quality factor value in each test was set to quite high values (between 2 and 2.5, depending on the available capacitor and inductor banks), in order to test the commercial anti-islanding techniques under the worst case scenario. High values of quality factor indicate that high amounts of reactive power are stored in the load compared to dissipated energy during a period. Thus, a high resonance at nominal grid frequency is achieved, making detection of the islanding more difficult.

For the non-linear load case, a diode rectifier with a smoothing capacitor was introduced. The diode rectifier was connected with a resistive load, which consumed almost 10% of the total PV produced power. A detailed description of each test can be found on the EriGrid website [54].

TABLE 3 Distinct harmonic components as a percentage of fundamental harmonic component

| | H2 | H3 | H4 | H5 | H6 | H7 | H8 | H9 | H10 | H11 | THD% |
|--------------------|------|------|----|------|----|-------|----|----|-----|-----|-------|
| Pure sine wave | 0 | 0 | 0 | 0 | 0 | 0 | 0 | 0 | 0 | 0 | 0 |
| Mildly distorted-1 | 0 | 2.5% | 0 | 3% | 0 | 2.5% | 0 | 0 | 0 | 2% | 5% |
| Mildly distorted-2 | 0 | 0.5% | 0 | 1.5% | 0 | 1.5% | 0 | 0 | 0 | 2% | 2.96% |
| Highly distorted-1 | 1.5% | 2.5% | 0 | 5% | 0 | 4% | 0 | 0 | 0 | 2% | 7.31% |
| Highly distorted-2 | 1% | 1% | 0 | 3% | 0 | 0.25% | 0 | 0 | 0 | 2% | 4.61% |

3.2 | Clustering algorithms and criteriaCluster analysis methodology

3.2.1 | k-means algorithm

The k-means clustering algorithm is an unsupervised hard clustering method, which assigns the n data objects x_1, \dots, x_n to a pre-defined number of exactly k clusters C_1, \dots, C_k . Initial verb clusters are iteratively reorganised by assigning each verb to its closest cluster (centroid) and recalculating cluster centroids until no further changes take place. Every cluster is represented by the mean value of its data points. The optimising criterion in the clustering process is the sum of squared error E between the objects in the clusters and their respective cluster centroids c_1, \dots, c_n as shown in Equation (2).

$$J = \sum_{j=1}^k \sum_{i=1}^{n_j} x_i^{(j)} - c_j \quad (2)$$

where $x_i^{(j)}$ is the i -th data point, which belongs to the j -cluster, c_j is the centre of the respective cluster (j) and n_j is the number of the data points in the respective cluster.

The k-means++ algorithm is sensitive to the selection of the initial partition, so the initialisation may vary. On the other hand, k-means++ imposes a Gaussian parametric design on the clustering result and generally tends to create compact clusters.

3.2.2 | Silhouette analysis

To obtain the silhouette value, S , in Equation (3) for an object within a cluster C_A as Equation (4) depicts, the average distance among all objects in this cluster is compared with the average distance b between every object in the neighbouring cluster C_B , according to Equation (5). For every simple object a value between $-1 < S < 1$ applies; if S is high, the average object distance within the cluster is smaller than the average distance of the objects in the neighbouring cluster, so the referred object is well classified. Otherwise, the referred object is misclassified.

$$S(y_j) = \frac{b(y_j) - a(y_j)}{\max\{a(y_j), b(y_j)\}} \quad (3)$$

$$a(y_j) = \frac{1}{|C_A| - 1} \sum_{y_i \in C_A, y_i \neq y_j} d(y_i, y_j) \quad (4)$$

$$b(y_j) = \min_{C_A \neq C_B} \frac{1}{|C_B|} \sum_{y_i \in C_B} d(y_i, y_j) \quad (5)$$

3.2.3 | WCBCR criterion

In order to evaluate k-means performance and seek the appropriate number of partitions, the WCBCR criterion is employed [38,39], as defined in Equation (6).

$$WCBCR = \frac{\sum_{k=1}^K \sum_{j=1}^N d^2(w_k, x_j)}{\sum_{1 \leq s < t \leq K} d^2(w_s, w_t)} \quad (6)$$

$w_t, w_s \in W_k$; W_k indicates the group that includes the centroids $W_k = \{w_k, k = 1, 2 \dots K\}$; N is the total number of the data set. In addition, $d(x, y)$ is the Euclidean distance norm. The denominator in Equation (6) involves the sum of the distances of all clusters between the respective centroids and the patterns, whereas the nominator measures the distances between the clusters. The optimal number of clusters is obtained by the lower value of the WCBCR index.

4 | EXPERIMENTAL RESULTS

4.1 | Results

In this subsection, the experimental results are briefly summarised to provide some generic conclusions regarding the impact of some key factors on the performance of anti-islanding algorithms. The experimental procedure was performed in a representative subset of the LV system assuming high PL of PVs and various disturbance factors. In connection to Section 3, it is noted that 1152 different tests were performed in order to cover all possible scenarios. In Figure 3 the results from the 3ph-commercial inverter evaluation are illustrated (individual operation). In more detail, Figure 3a presents the percentage of the total undetected island conditions (regardless of grid conditions), whereas Figure 3b–d present undetected islands' allocation under various grid conditions (grid impedance value, voltage distortion level, U/O frequency and/or voltage conditions, respectively). It is recalled that during these tests the quality factor values of the island circuit were set to quite high values (between 2 and 2.5).

In light of the above, it is concluded that the majority of undetected islands coincide with weak grid conditions, in a percentage which amounts to 71% as Figure 3b depicts (Z_1, Z_2 and Z_3 grid impedance cases). Furthermore, according to Figure 3c, it seems that voltage distortion at PCC does not affect the anti-islanding performance of the 3ph-inverter. Next, according to Figure 3d, fewer incidents of undetected islands occur during under voltage conditions. Last but not least, the presence of negative sequence at PCC voltage affects also the anti-islanding performance.

The same concept is followed in Figures 4 and 5 for the parallel operation of the 3ph-inverter with MICs and 1ph-inverters, respectively. Figures 4a and 5a outline that the parallel operation of the 3ph-inverter either with the 1ph-inverters or the MICs leads to a notable decrease of undetected islands number (compared with the individual operation of the 3ph-inverter). The influence of the negative sequence remains high either for the parallel operation of the 3ph-inverter and the MICs or of the 3ph-inverter and the 1ph-inverters (as shown in Figures 4d and 5d). Additionally, it is concluded that in the case of parallel operation of the 3ph-inverter and the MICs the number of undetected islands due to under/over voltage or

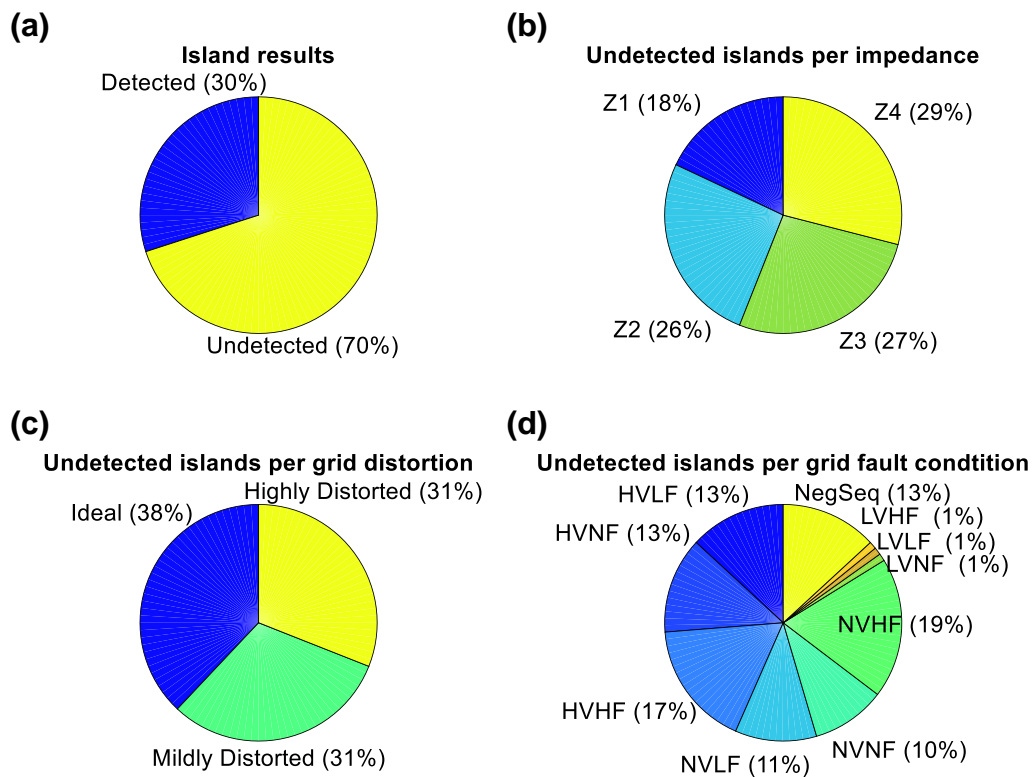


FIGURE 3 Undetected islanded conditions analysis (3-ph inverter individual operation, linear load)

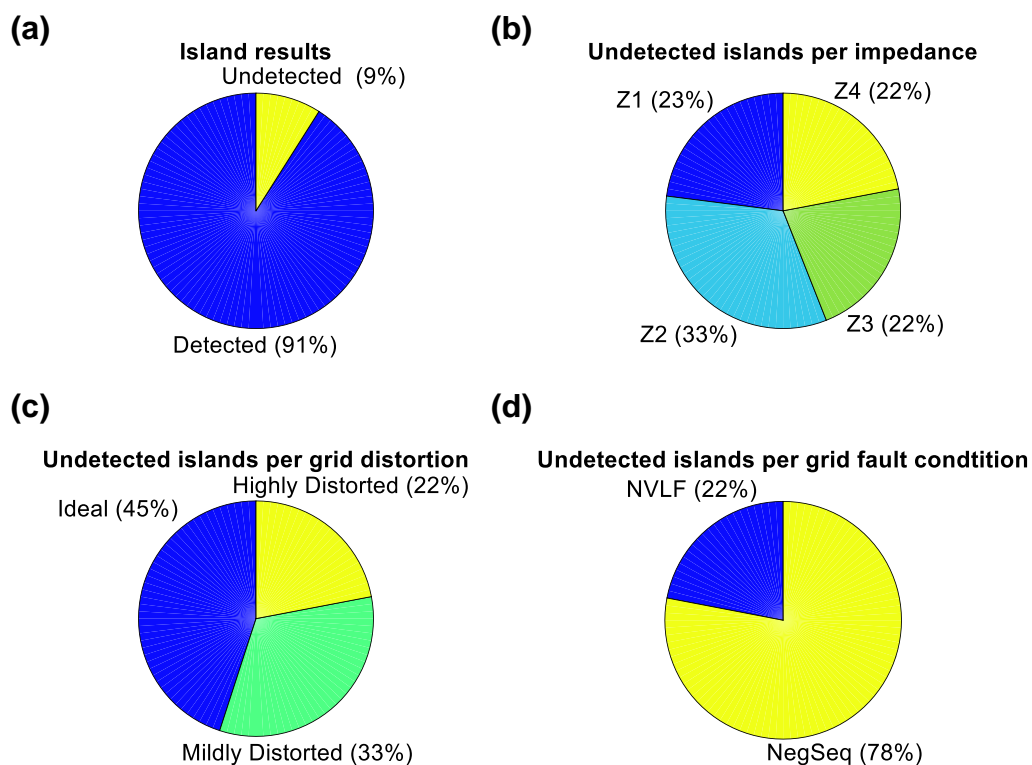


FIGURE 4 Undetected islanded conditions analysis (parallel operation of 3ph-inverter and MICs, linear load)

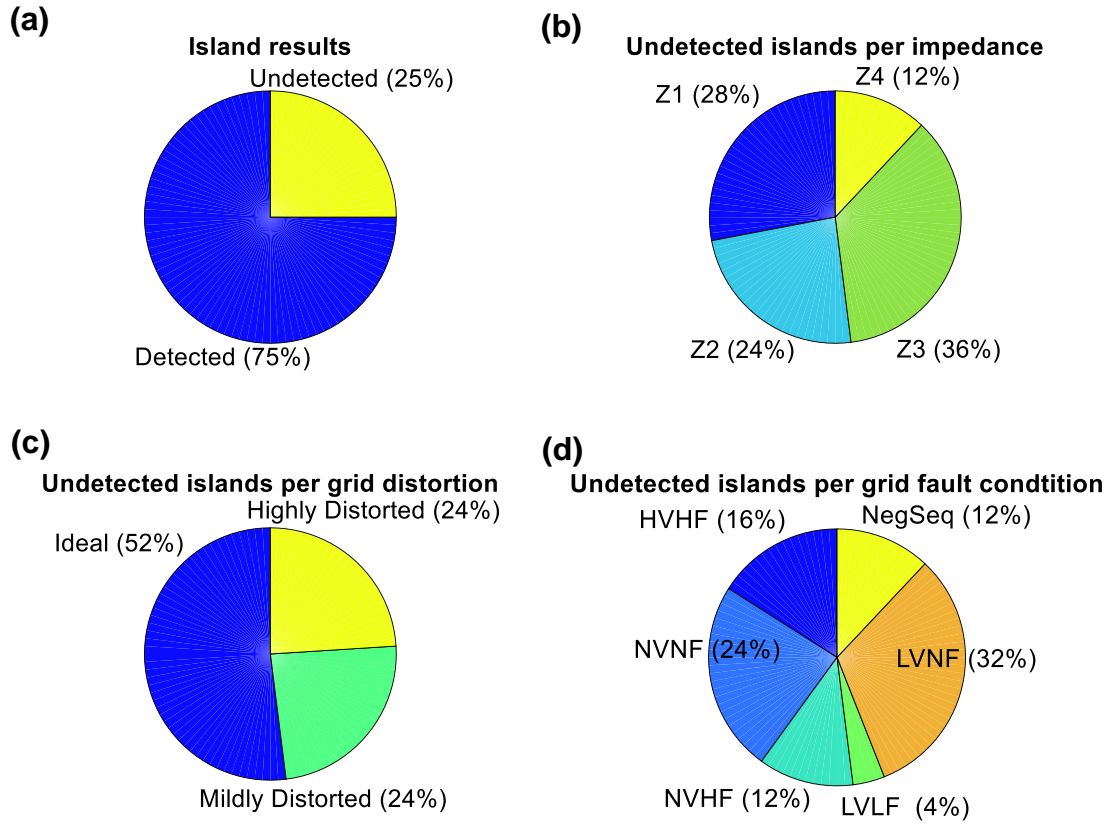


FIGURE 5 Undetected islanded conditions analysis (parallel operation of 3ph and 1ph inverters, linear load)

frequency events has been drastically decreased. This is due to the tight voltage and frequency limits of the 1ph-inverters.

Comparing Figures 3–5, the parallel operation of the 3ph-inverter either with the 1ph-inverters or the MICs increases the total number of detected islands, reducing the failure detection rate in stronger grids. In addition, a slight deterioration in anti-islanding performance of parallel operations under the ideal distortion level is observed, followed by an improved response in highly distorted grids.

The results of the parallel operation of all the available inverters are illustrated in Figures 6 and 7 for linear and non-linear load, respectively. It is noted that the total amount of undetected islands in Figure 6 is roughly the same as those in Figure 5, where linear load conditions also are considered; consequently, the operation of MICs does not affect the amount of undetected islands. As is reasonable, most of the undetected cases occur under weak grid conditions, whereas the outcomes of Figures 4 and 5 are also valid for these cases. It is crucial to note that in the last scenario (in which all the inverters are operating in parallel under non-linear load) the impact of the negative sequence is eliminated.

Examining the results of Figures 6 and 7, it is observed that in the case of non-linear load there is a significant increase in successful island detection. It is also noted that higher levels of harmonic distortion along with non-linear load tend to improve the anti-islanding performance of inverters parallel operation.

4.2 | Descriptive statistical analysis

Descriptive statistical analysis is used to summarise a set of observations, in order to manage a huge amount of data in a quick and concise manner [55]. This type of statistical analysis was deemed necessary in order to organise the large amount of collected data and outline a strategy for further analysis. The results of the descriptive analysis are listed in Table 4. This table shows the results of all possible combinations of the inverters under test, both for linear and non-linear loads. It can be concluded that the 1ph-inverters and MICs have successfully detected islanded conditions in their individual operation mode, for any grid and load conditions. On the other hand, the 3ph-inverter in individual operation has a significant high-undetected rate (about 70%). Additionally, it is highlighted that the combination of the 3ph and the 1ph inverters reduces significantly the total number of undetected islands. It is also noted that the combination of all the inverters has failed to detect islanded conditions by a percentage of 54% and 28% in linear and non-linear load cases, respectively.

4.3 | Box plot analysis

In descriptive statistical analysis, the boxplot is a standardised way of displaying graphically the distribution of data based on a five-number summary of a set of data (minimum, first

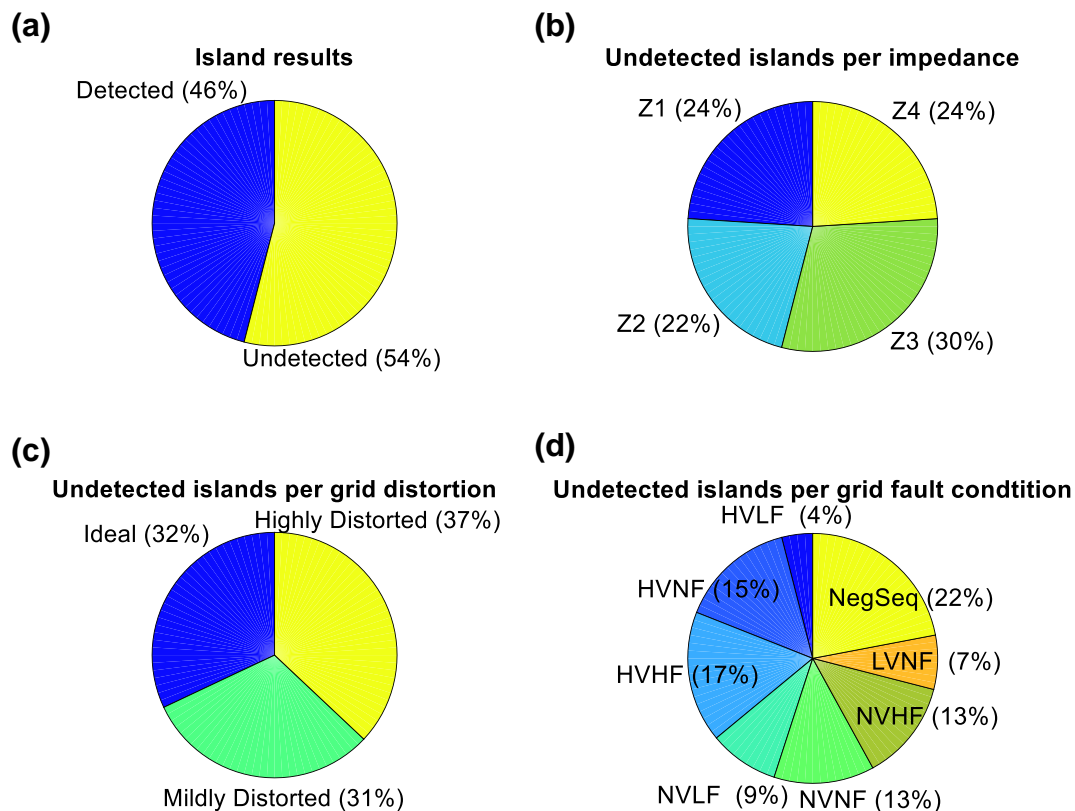


FIGURE 6 Undetected islanded conditions analysis (all inverters in operation, linear load)

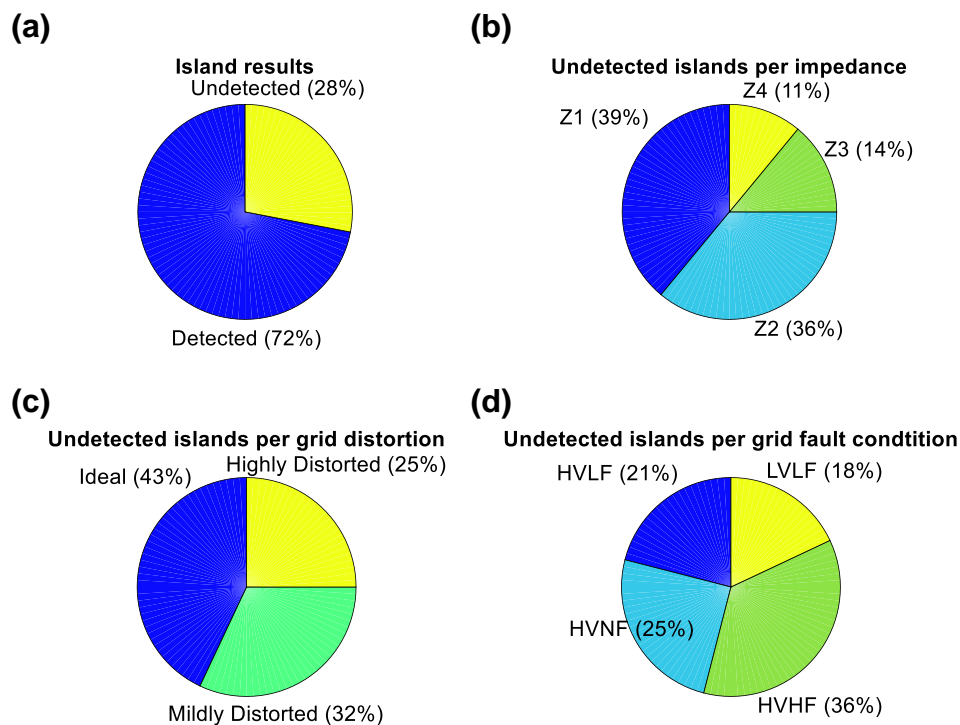


FIGURE 7 Undetected islanded conditions analysis (all inverters in operation, non-linear load)

| Combination of Inverters | Total (%) | | Undetected | | | | | | |
|---------------------------|-----------|------------|---------------|-------|-------|-------|----------------|----|----|
| | Detected | Undetected | Impedence (%) | | | | Distortion (%) | | |
| | | | Z_1 | Z_2 | Z_3 | Z_4 | ID | MD | HD |
| 3ph-inverter | 30 | 70 | 18 | 26 | 27 | 29 | 38 | 31 | 31 |
| 1ph-inverter | 100 | 0 | - | - | - | - | - | - | - |
| MICs | 100 | 0 | - | - | - | - | - | - | - |
| 3ph-MICs | 91 | 9 | 23 | 33 | 22 | 22 | 45 | 33 | 22 |
| 3ph-1ph | 75 | 25 | 28 | 24 | 36 | 12 | 52 | 24 | 24 |
| 1ph-MICs | 100 | 0 | - | - | - | - | - | - | - |
| 3ph-1ph-MICs | 46 | 54 | 24 | 22 | 30 | 24 | 32 | 31 | 37 |
| 3ph-1ph-MICs (non-linear) | 72 | 28 | 39 | 36 | 14 | 11 | 43 | 32 | 25 |

TABLE 4 Total descriptive statistical analysis of all cases

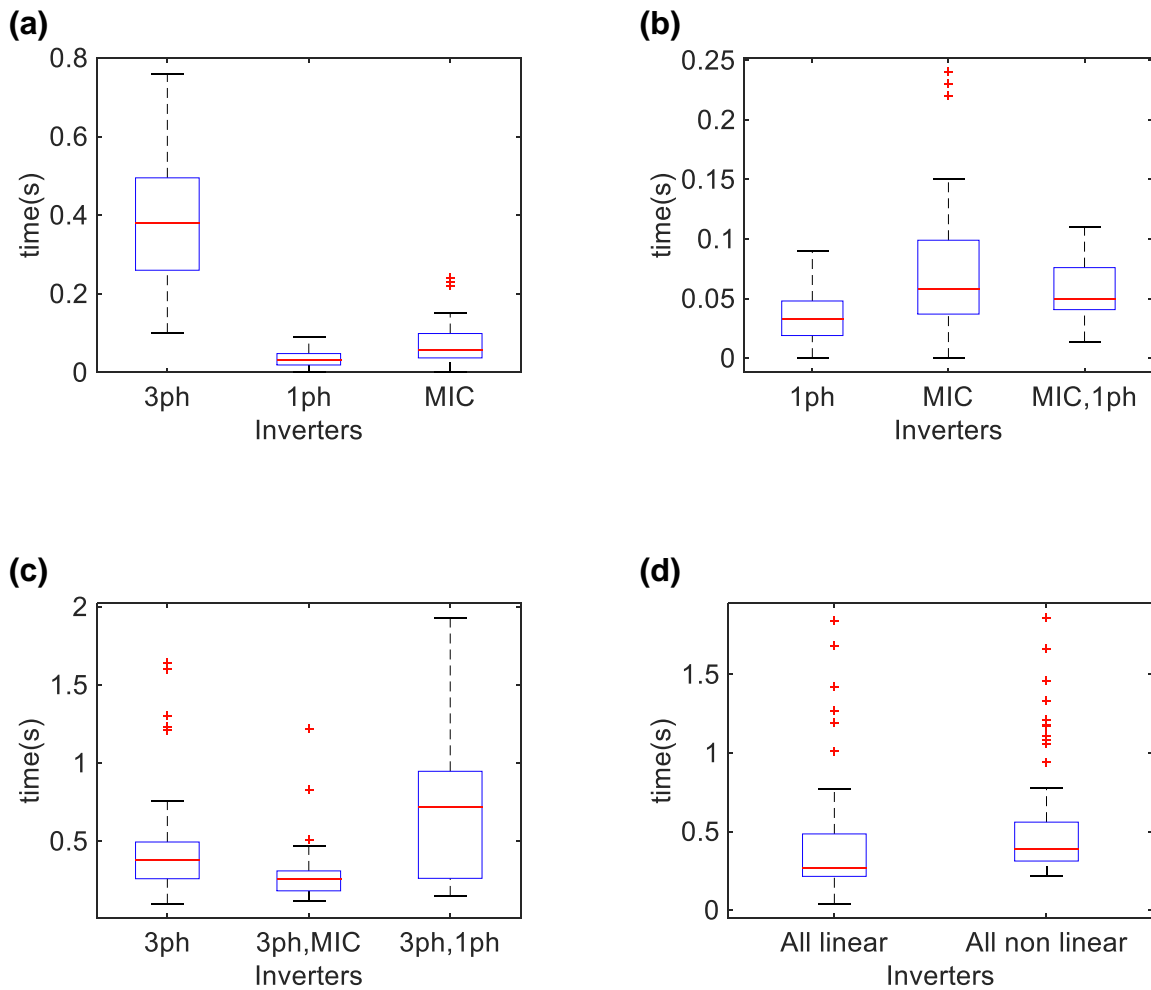


FIGURE 8 Box plot analysis of all cases, (a)–(c) linear load and (d) all inverters under linear and non-linear load, respectively

quartile, median, third quartile and ‘maximum’) [56]. In this case, the boxplot approach can indicate some meaningful information regarding the distribution, the outliers, the mean, the median and the variance of the inverters anti-islanding protection time response. The maximum specified time for island detection is set by international standards [42,43]. According to

those standards a PV inverter complies with the requirements for islanding protection when it detects the island and ceases its operation in less than 2 s.

Figure 8a shows the boxplot scheme of each inverter type under sole operation. In Figure 8b, the parallel operation of the 1ph-inverters and MICs is compared with their sole

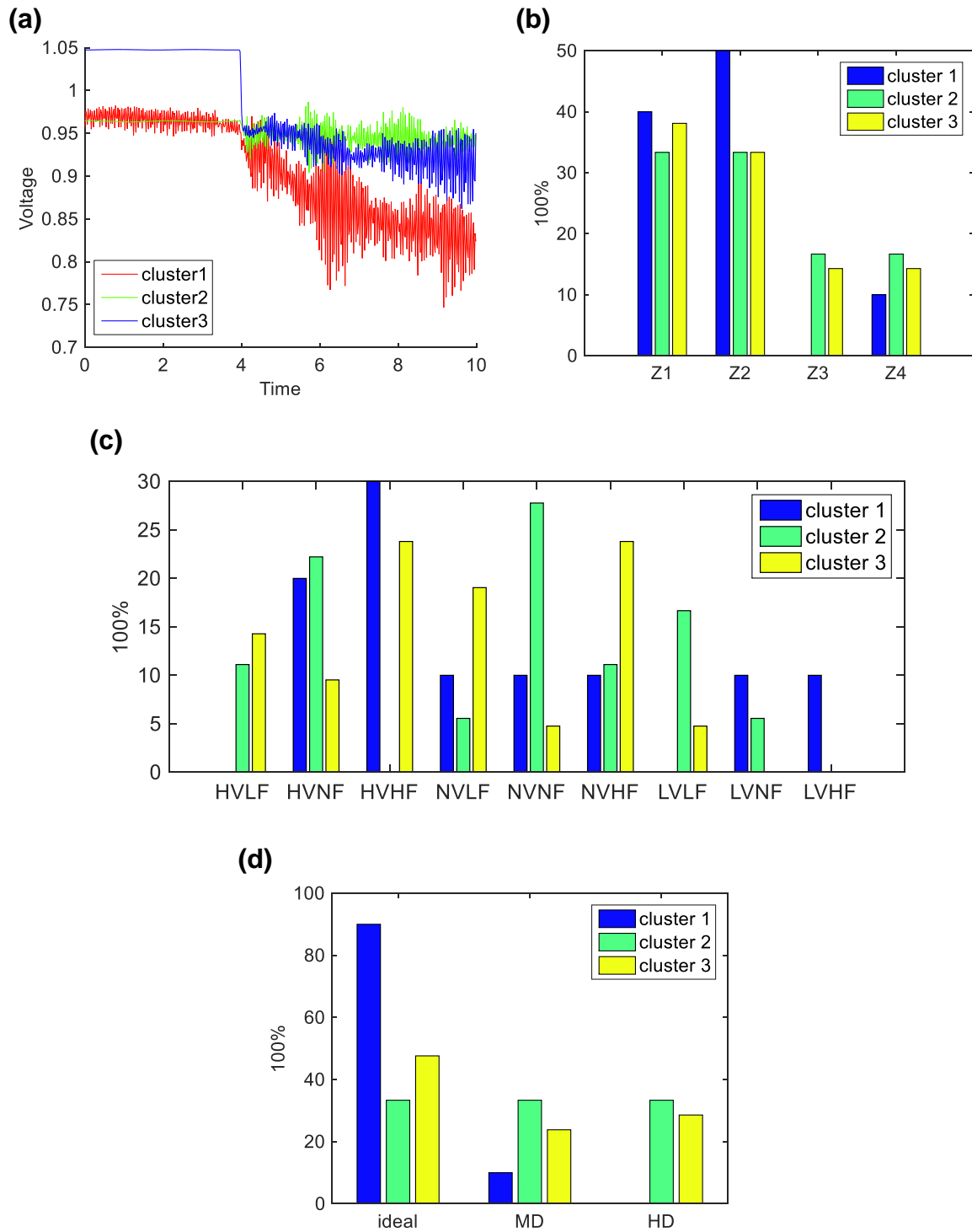


FIGURE 9 Clustering analysis of rms voltage waveform (a) and synthesis of clusters (b)–(d)

operation. In Figure 8c, the boxplot of the individual operation of the 3ph-inverter is compared either to its parallel operation with the 1ph-inverters or MICs. It is highlighted that the parallel operation of the 3ph-inverter and MICs reduces the median time response of the 3ph-inverter. On the other hand, the parallel operation of 3ph- and 1ph-inverters leads to an increase in the total time response to islanded

conditions, whereas the upper whisker of the combined case is approaching the limit of 2 s; the interquartile range of this case is 0.7 s. Figure 8d illustrates the boxplots for the case that all the inverters operate in parallel to the PCC, both for linear and non-linear load conditions. It is noted that the operation under non-linear load increases the total time response of the inverters in comparison with their response

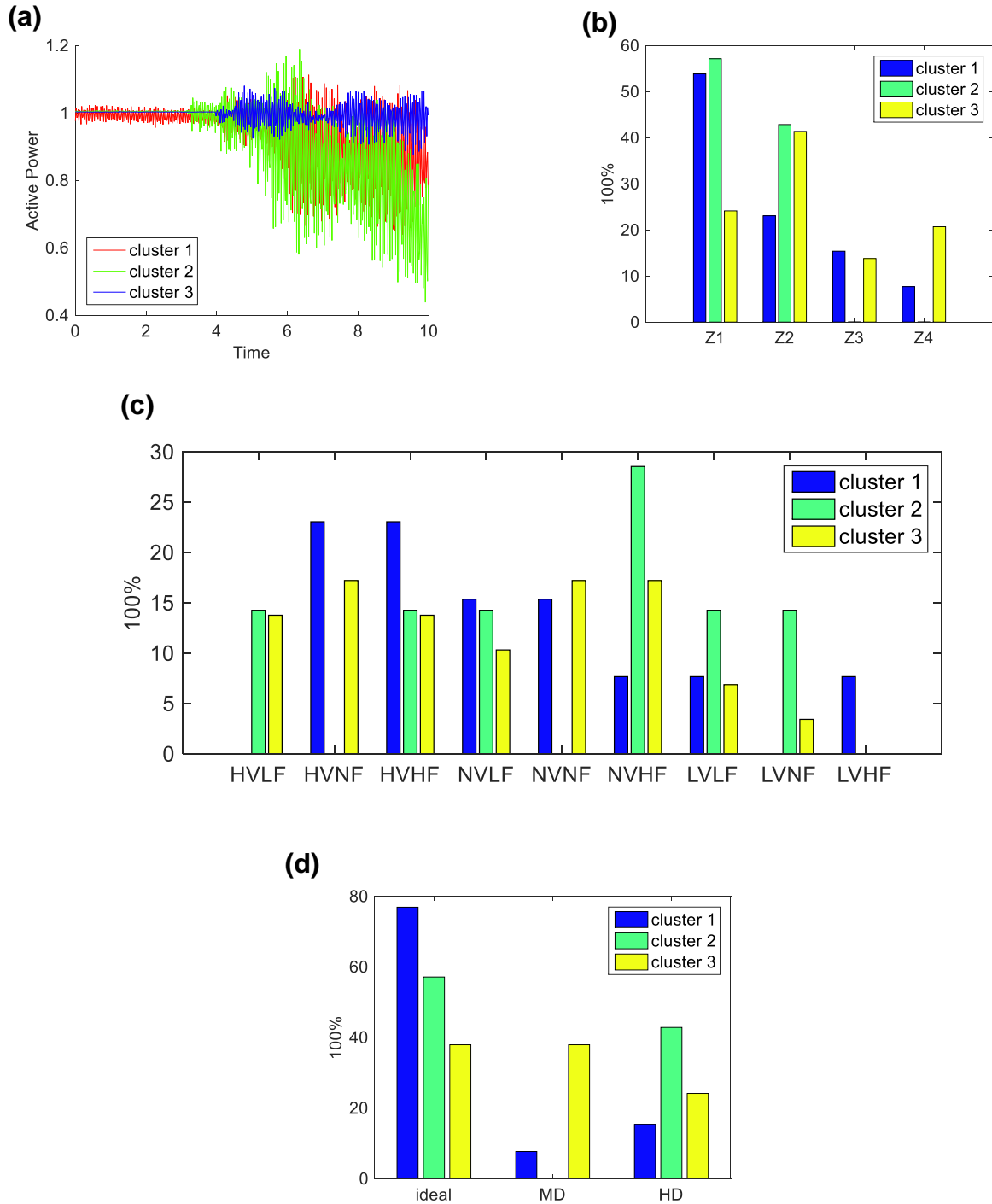


FIGURE 10 Clustering analysis of active power waveform (a) and synthesis of clusters (b)–(d)

under linear load; however, the negative skew remains in both cases.

The outliers of the non-linear case have a significant accumulation inside the zone of 1–1.2 s. This can be justified by the fact that the total number of undetected cases is significantly reduced and many of the undetected cases under linear load are now successfully located within the permissible time frame.

5 | CLUSTER ANALYSIS

5.1 | 3ph-inverter

According to the analysis in the previous section, the 3ph-inverter determines the vast number of undetected islands, under any line and load conditions. Hence, the present cluster analysis focuses on the operation of this inverter. In this

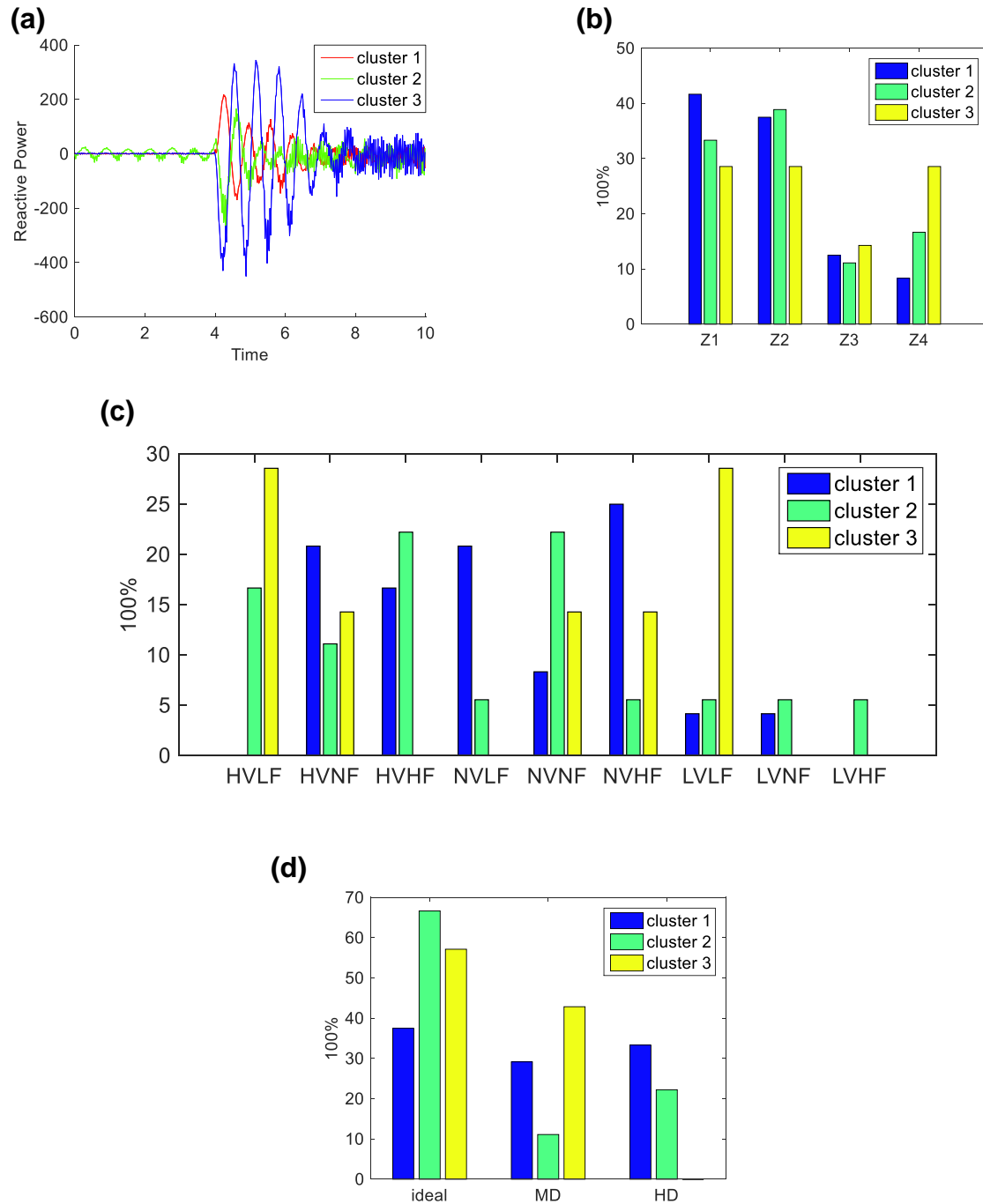


FIGURE 11 Clustering analysis of reactive power waveform (a) and synthesis of clusters (b)–(d)

context, Figures 9–12 illustrate the comparison of k-means++ algorithm results for the individual operation of the 3ph-inverter. The test parameters that constitute the base of the clustering segregation are the following: the rms voltage, the frequency, and the active and reactive power at PCC. These are the four parameters of the silhouette plot that ensure a smarter initialisation of the centroids and improve the quality of the clustering for the k-means++ algorithm.

The selection of the number of clusters was based on the Silhouette plots and WCRBR criteria, as already discussed. Additionally, the factors that affect the formation of the

abovementioned clusters are presented in the same figures (allocation of grid impedance, U/O voltage and/or frequency, as well as voltage distortion level). Considering the vast amount of collected data, it was imperative to categorise them by their distinguishing features.

The participation factors for each cluster, considering the 3ph-inverter individual operation, are listed in Table 5. For this specific case of operation, the clustering analysis of the selected parameters and the corresponding synthesis of clusters are depicted in Figures 9–12. According to those figures, three patterns are formed for each selected parameter. In addition,

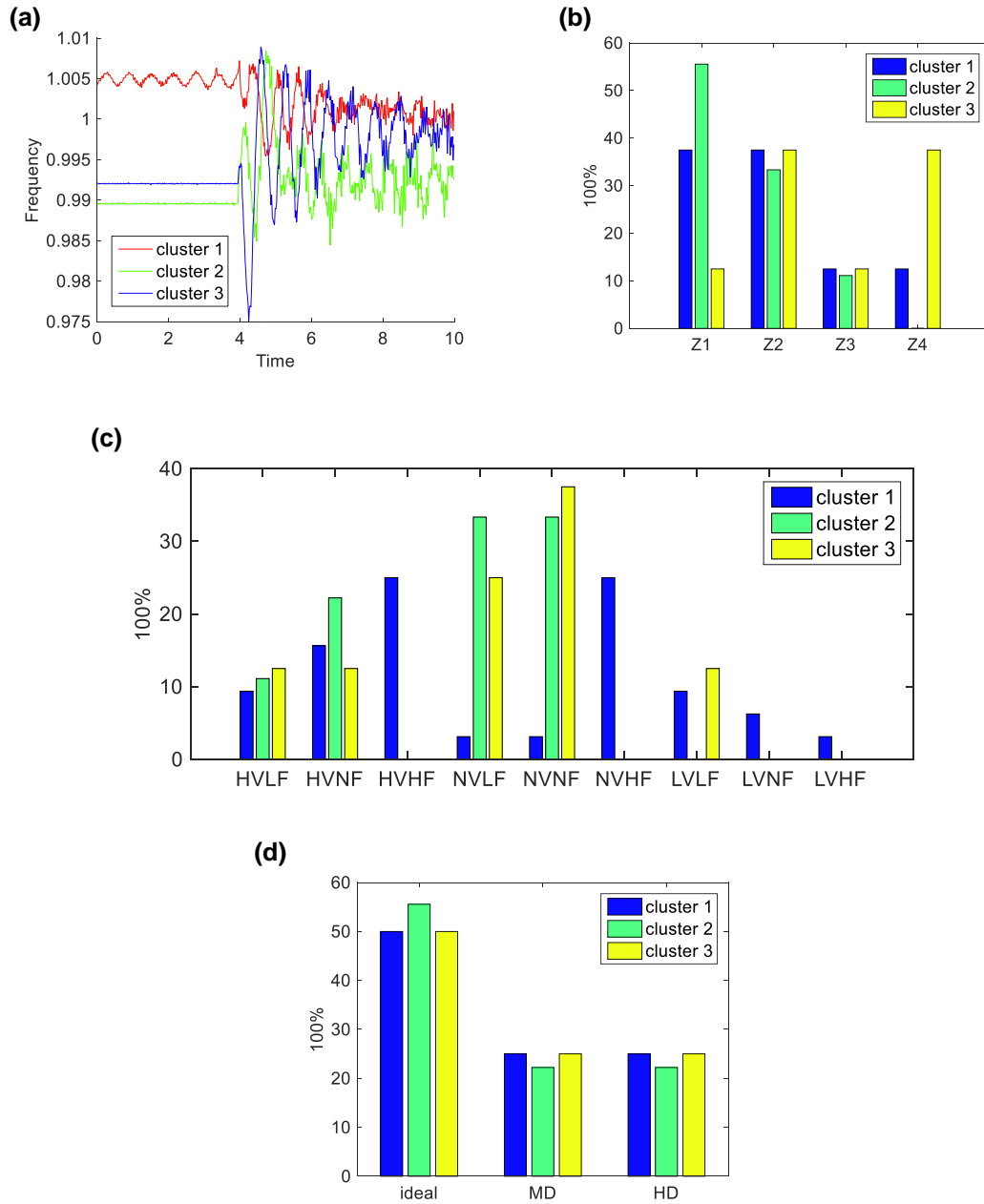


FIGURE 12 Clustering analysis of frequency waveform (a) and synthesis of clusters (b)–(d)

| Participation factor (%) | Cluster #1 | Cluster #2 | Cluster #3 | Mean value |
|--------------------------|------------|------------|------------|------------|
| rms voltage | 20.4 | 36.7 | 42.9 | 254 V |
| Active power | 26.5 | 14.3 | 59.2 | 4071 W |
| Reactive power | 49 | 36.7 | 14.3 | 38.8 var |
| Frequency | 66 | 18.4 | 15.6 | 50.1 Hz |

TABLE 5 Participation factors of the selected parameters for the individual operation of the 3ph-inverter

subfigures (b) in Figures 9–12 highlight the vulnerability of the 3ph-inverter anti-islanding protection in weak grids, whereas subfigures (c) and (d) prove that the combined voltage and frequency unbalances deteriorate the inverter anti-islanding response regardless of the grid distortion level.

By observing Figure 10a, it is deduced that cluster #2 of the active power waveforms presents a particularly different formation compared to the remaining clusters, presenting a high rate of flickering and abrupt reduction of active power. However, Table 5 reveals that this cluster corresponds to a

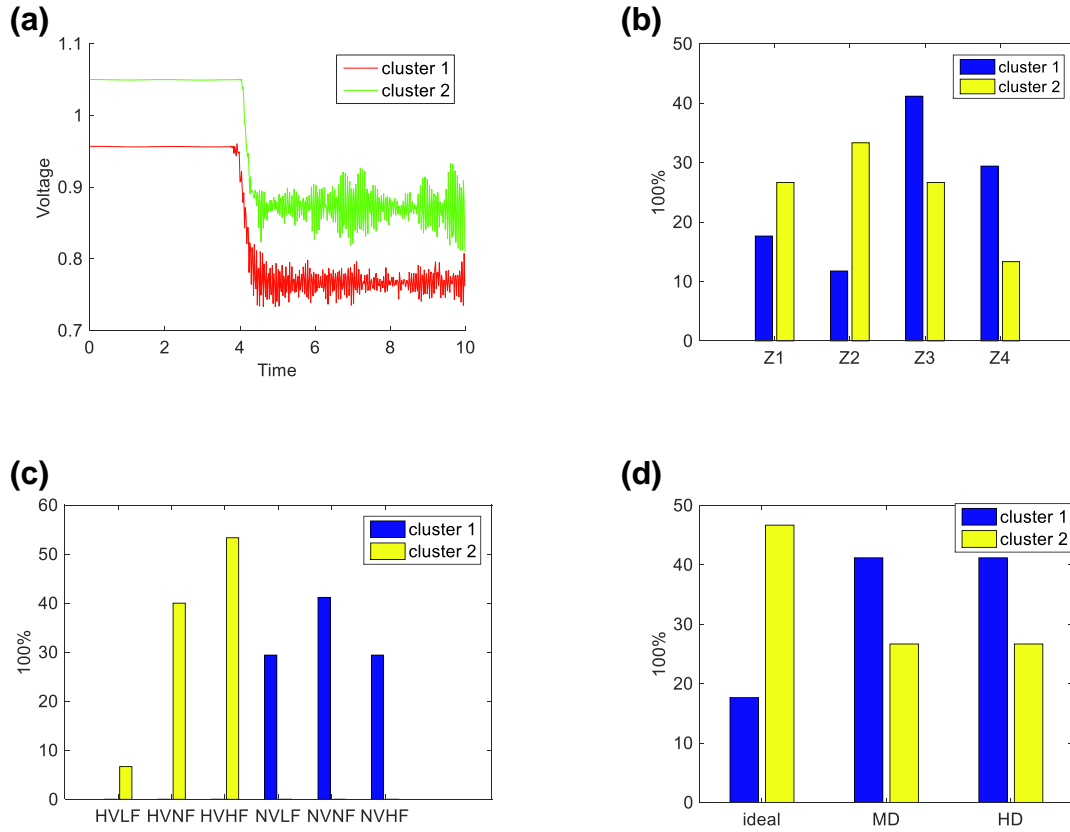


FIGURE 13 Clustering analysis of rms voltage waveform (a) and synthesis of clusters (b)–(d) (parallel operation of all the inverters, linear load)

relatively small percentage of the available data, thus it is of less importance. The same stands for the waveform of cluster #3 of the reactive power data (Figure 11a).

Additionally, in the (c) subfigures of Figures 9–12 the percentages of over/under voltage and over/under frequency cases are presented, leading to a failure response of the anti-islanding methods.

5.2 | Parallel operation of all available inverters under linear load

In Figures 13–16 the comparison of k-means++ algorithm results are depicted for the parallel operation of all available inverters. Additionally, the factors that affect the formation of the above-mentioned clusters are presented in the same figures (allocation of grid impedance, U/O voltage and/or frequency, as well as voltage distortion level). In this case, the optimum number of clusters was two, according to the response during island events, based on Silhouette and WCRBR criteria. As in the previous section, the test parameters that constitute the base of the clustering segregation are the following: the rms voltage, the frequency, the active and the reactive power at PCC.

The implementation of the k-means++ algorithm reveals significant differences in the waveforms of the rms voltage, active power and frequency. The participation factors for each

cluster, considering the parallel operation of all available inverters under linear load, are listed in Table 6. Initially, the step response of voltage and active power waveforms, in Figures 13a and 14a, respectively, reveals that 1ph-inverters and MICs cease their operation whilst the 3ph-inverter continues, so failing to detect the island condition.

Moreover, subfigures (b) of Figures 13–16 along with subfigures (d) of Figures 3–5, indicate that MICs involvement in a parallel operating scheme eliminates failures in the case of under voltage/frequency conditions. Finally, according to Figure 13c, the clusters of rms voltage waveform stand for high and normal voltage levels, respectively.

5.3 | Parallel operation of all available inverters under non-linear load

In Figures 17 and 18, the comparisons of k-means++ algorithm results (reactive power and frequency) are depicted for the parallel operation of all available inverters under non-linear load. Additionally, the factors that affect the formation of the above-mentioned clusters are presented in the same figures (allocation of grid impedance, U/O voltage and/or frequency, as well as voltage distortion level). The Silhouette and WCRBR criteria have shown that there is no suggested number of clusters for the rms voltage and active power cases. However, it is worth noting that in the

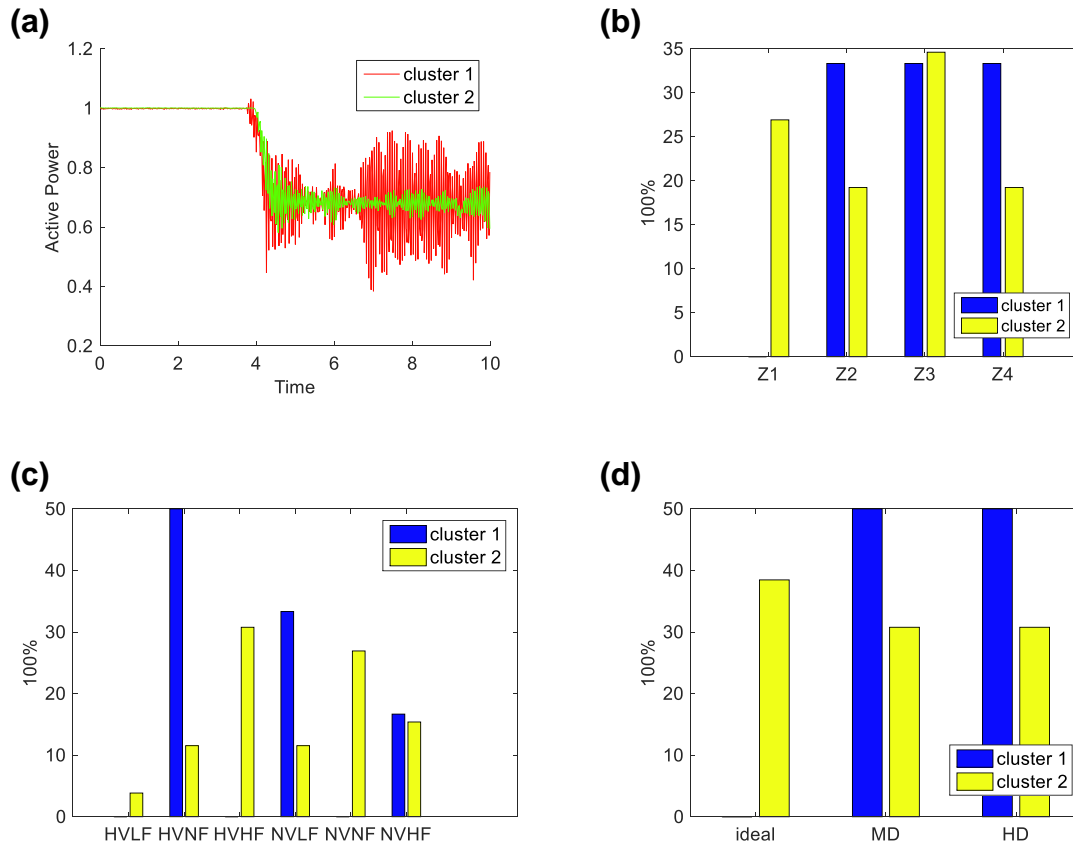


FIGURE 14 Clustering of active power waveform (a) and synthesis of clusters (b)–(d) (parallel operation of all the inverters, linear load)

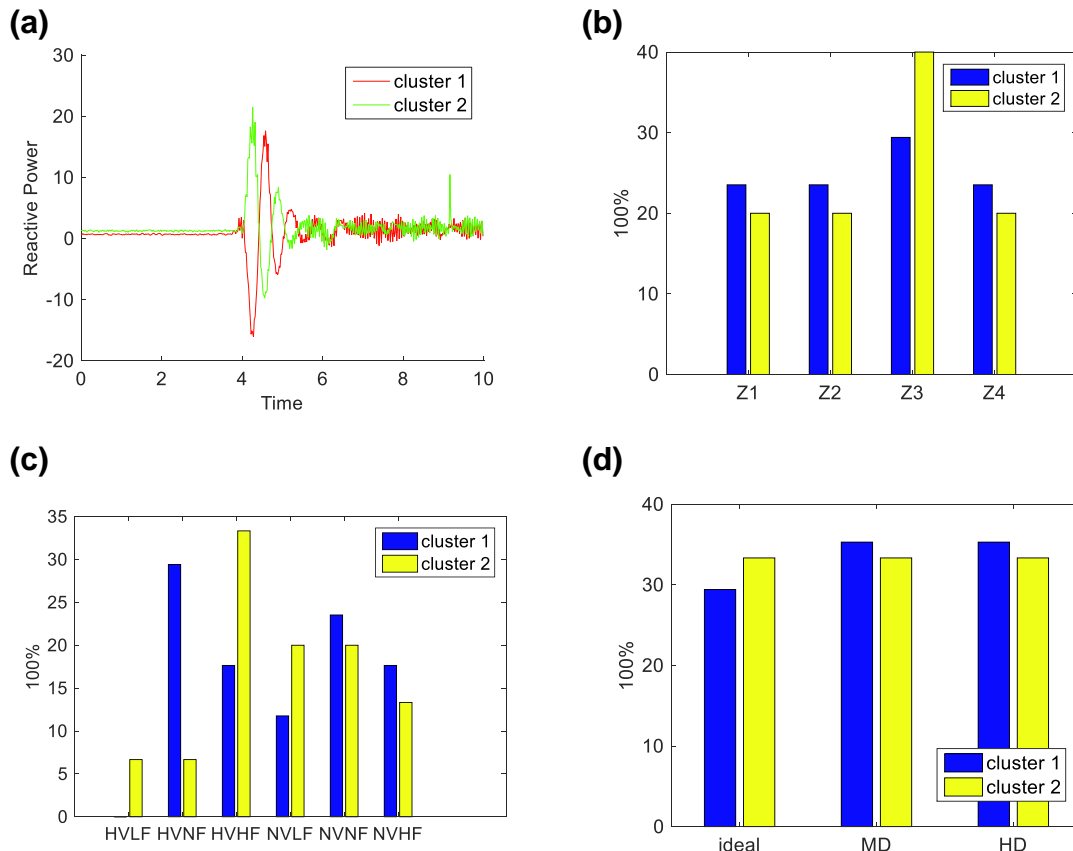


FIGURE 15 Clustering analysis of reactive power waveform (a), and synthesis of clusters (b)–(d) (parallel operation of all the inverters, linear load)

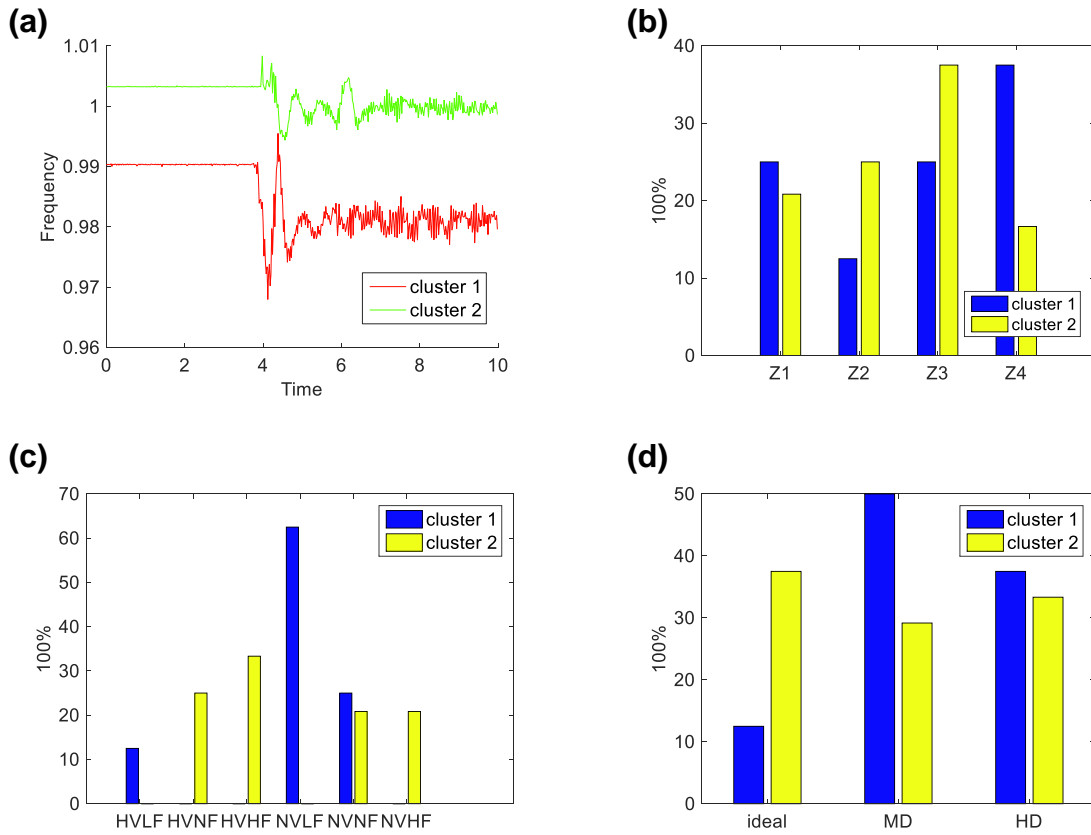


FIGURE 16 Clustering analysis of frequency waveform (a) and synthesis of clusters (b)–(d) (parallel operation of all the inverters, linear load)

TABLE 6 Participation factors of the selected parameters for parallel operation of all available inverters under linear load

| Participation factor (%) | Cluster #1 | Cluster #2 | Mean value |
|--------------------------|------------|------------|------------|
| rms voltage | 53.1 | 46.9 | 242 V |
| Active power | 18.8 | 81.2 | 4085 W |
| Reactive power | 53.1 | 46.9 | 29.5 var |
| Frequency | 25 | 75 | 50 Hz |

waveforms of rms voltage and active power the step response remains the same as in the linear load case. This indicates that the 3ph-inverter continues its operation uninterruptedly (although island conditions exist), while the 1ph-inverters and MICs successfully cease their operation. The participation factors for each cluster, considering the parallel operation of all available inverters under non-linear load, are listed in Table 7.

Analysing the waveforms of reactive power and frequency it is concluded that the optimum number of clusters is two, based on Silhouette and WCRBR criteria. The implementation of the k-means++ algorithm has revealed significant differences in the waveforms of the frequency and reactive power.

By observing Figures 17 and 18 and Table 7, it is revealed that there is no notable variation between those two individual

clusters. Compared with the previous subsection, less voltage and active power fluctuations were observed, due to the nature of the non-linear load. As for the waveform of the reactive power that Figure 17 illustrates, the weaker the grid, the more intense the reverse reactive power flow. Additionally, from Figures 17 and 18 it can be deduced that for the parallel operation of all available inverters under linear load the over voltage grid condition has a notable impact on the successful islanding detection.

6 | CONCLUSION

A comprehensive investigation of commercial inverters islanding prevention measures has been presented, with the prospect of mass PL increase of PVs, where multiple inverters are connected to the same PCC. Various combinations of the available inverters were studied, and their responses were categorised by using advanced mathematical criteria. In this context, clustering analysis was used to identify the real impact of every system parameter, that is, grid impedance, grid distortion and H/L V or H/L F conditions.

According to the experimental results, the performance of anti-islanding protection schemes is greatly affected by the prospect of high PL of single-phase PV systems. In addition, it has been deduced that active anti-islanding methods that

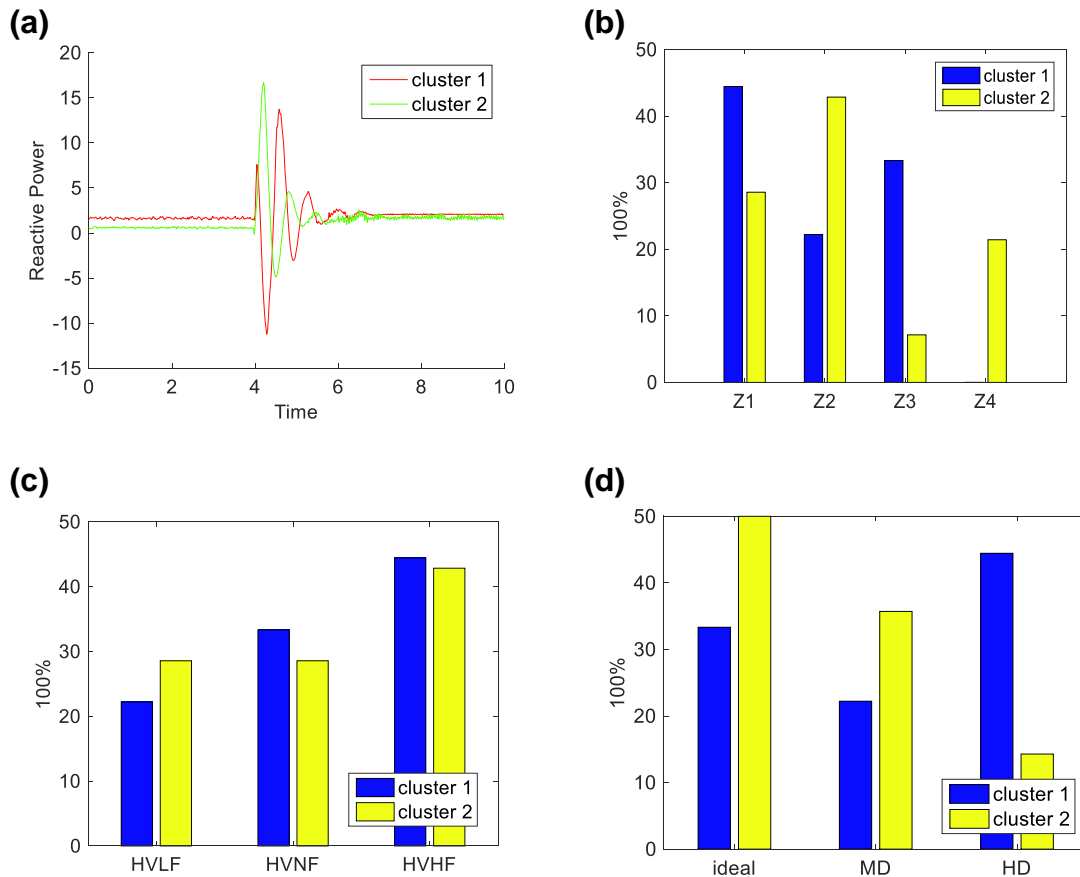


FIGURE 17 Clustering analysis of reactive power waveform (a) and synthesis of clusters (b)–(d) (parallel operation of all the inverters, non-linear load)

employ reactive current components may fail to detect the island under high-quality factor values, as the reactive current is limited by power quality standards. In addition, most of the islanded conditions that were undetected regarded strong grid conditions. Apparently, this was due to the anti-islanding algorithm of the inverter and its dependence on the short circuit level at the PCC.

For the above reasons, the incorporation of more sophisticated active anti-islanding techniques is of high importance in order to overcome the above limitations; the higher order harmonic injection [57] or active cross-correlation anti-islanding schemes [58] could pave the way for higher PL of PVs in the LV distribution network.

As regards voltage harmonic distortion, although it was kept within the acceptable limits, it seems that several issues emerge regarding the interconnection of the commercial inverters with the grid. In some cases, the inverter failed to reach its nominal power, whereas in other cases (where the grid was mildly or highly distorted) the inverter failed to connect to the grid.

As regards the parallel operation of multiple inverters, as has been already noted, the detection time was significantly extended in comparison with both the 3ph- and 1ph-inverters individual operation. Finally, the parallel operation of all available inverters resulted in a decrease of the median time

value of the detected island events in comparison with the 3ph-inverter individual operation.

The presence of non-linear loads results in less unsuccessful island detections. This outcome shows that the implementation of strict power quality improvement techniques at load side might have a negative impact on the performance of anti-islanding algorithms under high PL of PVs.

In addition, the results of cluster analysis were essential for this investigation, providing insightful conclusions for the cases of false operation (undetected islanded cases). In more detail, cluster analysis has revealed that for the undetected cases under linear load the parameters that have high impact on voltage waveforms are the harmonic distortion and the overvoltage level, accompanied by over/under frequency conditions. An additional outcome from cluster analysis is that the increased PL and the harmonic distortion are the main factors that affect the fluctuation of real power in undetected events. Nevertheless, those active power fluctuations are not capable of activating the anti-islanding protection schemes of the inverters under test.

Last but not least, the fact that anti-islanding protection is a key issue for the achievement of high PL of PVs in LV distribution networks has been highlighted. The existing anti-islanding algorithms are not designed for such a network

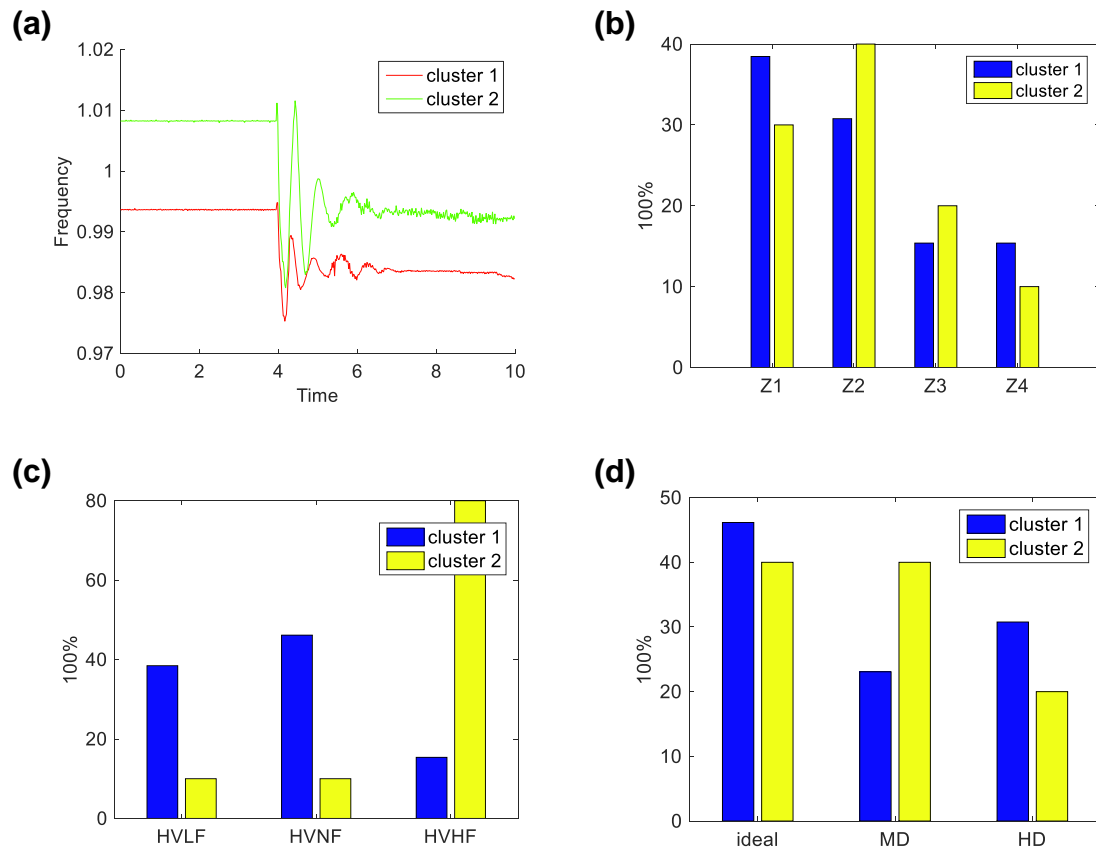


FIGURE 18 Clustering analysis of frequency waveform (a) and synthesis of clusters (b)–(d) (parallel operation of all the inverters, non-linear load)

TABLE 7 Participation factors of the selected parameters for the parallel operation of all available inverters under non-linear load



| Participation factor (%) | Cluster #1 | Cluster #2 | Mean value |
|--------------------------|------------|------------|------------|
| rms voltage | — | — | 254 V |
| Active power | — | — | 4071 W |
| Reactive Power | 39.1 | 60.9 | 34.8 var |
| Frequency | 56.5 | 43.5 | 50.1 Hz |

development, hence new and more advanced algorithms need to be employed by commercial inverters, as referred to previously in [57,58]. In addition, more detailed test procedures for the evaluation of anti-islanding techniques have to be adopted, taking into account the network parameters at PCC [59].

ACKNOWLEDGEMENT

This work was supported in part by the European Commission within the Horizon 2020 framework ERIGrid project under Grant agreement 654113.

ORCID

Anastasios Kyritsis  <https://orcid.org/0000-0003-1348-1395>
 Nick Papanikolaou  <https://orcid.org/0000-0001-8546-1196>

REFERENCES

1. Dietmannsberger, M., Schulz, D.: Impacts of low-voltage distribution grid codes on ancillary services and anti-islanding detection of inverter-based generation. *IEEE Trans. Energy Conv.* 31(4), 1287–1294 (2016)
2. El-naggar, A., Erlich, I.: Control approach of three-phase grid connected PV inverters for voltage unbalance mitigation in low-voltage distribution grids. *IET Renew. Power Gener.* 10(10), 1–9 (2016)
3. Eftekharijrad, S., et al.: Impact of increased penetration of photovoltaic generation on power systems. *IEEE Trans Power Syst.* 28(2), 893–901 (2013)
4. Kyritsis, A., et al.: Evolution of PV systems in Greece and review of applicable solutions for higher penetration levels. *Renew. Energy.* 109, 487–499 (2017)
5. Serban, E., Ordonez, M., Pondiche, C.: Voltage and frequency grid support strategies beyond standards. *IEEE Trans. Power Electron.* 32(1), 298–309 (2017)
6. Datta, A., et al.: Evaluation of anti-islanding techniques for renewable energy powered distributed generators using analytic network process. *IET Renew. Power Gener.* 10(9), 1–10 (2016)
7. Reigosa, D., et al.: Active islanding detection using high-frequency signal injection. *IEEE Trans Ind Appl.* 48(5), 1588–1597 (2012)
8. Reigosa, D., et al.: Active Islanding detection for multiple parallel-connected inverter-based distributed generators using high frequency signal injection. In: 2012 IEEE Energy Convers. Congr. Expo, ECCE 2012, pp. 2719–2726. (2012)
9. Zhou, Y., Li, H., Liu, L.: Integrated autonomous voltage regulation and islanding detection for high penetration PV applications. *IEEE Trans. Power Electron.* 28(6), 2826–2841 (2013)
10. Velasco, D., et al.: Review of anti-islanding techniques in distributed generators. *Renew. Sustain. Energy Rev.* 14(6), 1608–1614 (2010)

11. Ropp, M., Begovic, M., Rohatgi, A.: Determining the relative effectiveness of islanding prevention techniques using phase criteria and non-detection zones. *IEEE Trans. Energy Convers.* 15(3), 290–296 (2000)
12. Bower, W., Robb, M.: Evaluation of islanding detection methods for utility-Interactive inverters in photovoltaic systems. SANDIA Rep. (2002)
13. Funabashi, T., Koyanagi, K., Yokoyama, R.: A review of islanding detection methods for distributed resources *IEEE Bol. PowerTech - Conf. Proc.*, 2, 608–613 (2003)
14. Kyritsis, A., et al.: Islanding detection methods for distributed PV systems overview and experimental study. *Energy Syst.* 63–79 (2016)
15. Bakhshi, M., Noroozian, R., Gharehpetian, G.B.: Anti-islanding scheme for synchronous dg units based on tufts-kumaresan signal estimation method. *IEEE Trans. Power Deliv.* 28(4), 2185–2193 (2013)
16. Dietmannsberger, M., Grumm, F., Schulz, D.: Simultaneous implementation of LVRT Capability and anti-islanding detection in three-phase inverters connected to low-voltage grids. *IEEE Trans. Energy Convers.* 32(2), 505–515 (2017)
17. Yan, R., Tapan, K.: Investigation of voltage stability for residential Customers due to high photovoltaic penetrations. *IEEE Trans. Power Syst.* 27(2), 651–662 (2012)
18. Yafaoui, A., Wu, B., Kouro, S.: Improved active frequency drift anti-islanding detection method for grid connected photovoltaic systems. *IEEE Trans. Power Electron.* 27(5), 2367–2375 (2012)
19. California energy commission. (2017). http://ww2.energy.ca.gov/electricity_analysis/rule21/documents/phase3. Accessed 12 June 2017
20. Photovoltaics, D.G., Storage, E.: IEEE Standard for Interconnection and Interoperability of Distributed Energy Resources with Associated Electric Power Systems Interfaces, pp. 1547–2018. IEEE, Piscataway, NJ (2018)
21. Teoh, W.Y.T., Tan, C.W.: An overview of islanding detection methods in photovoltaic systems. *World Acad. Sci. Eng. Technol.* 5(10), 674–682 (2011)
22. Liserre, M., et al.: An anti-islanding method for single-phase inverters based on a grid voltage sensorless control. *IEEE Trans. Ind. Electron.* 53(5), 1418–1426 (2006)
23. Cardenas, A., Agbossou, K.: Experimental evaluation of voltage positive feedback based anti-islanding algorithm: multi-inverter case. *IEEE Trans. Energy Convers.* 27(2), 498–506 (2012)
24. Hoke, A.F., et al.: An islanding detection test Platform for multi-inverter islands using power HIL. *IEEE Trans Ind Electron.* 65(10), 7944–7953 (2018)
25. Narendra Babu, P., et al.: An optimal current control scheme in grid-tied hybrid energy system with active power filter for harmonic mitigation. *Int. Trans. Electr. Energy Syst.* 30(3), 1–21 (2020)
26. Kumar, V.N., et al.: Improved power quality in a solar PV plant integrated utility grid by employing a Novel Adaptive current regulator. *IEEE Syst. J.* 1, 1–12 (2019)
27. Narendra Babu, P., Peesapati, R., Panda, G.: An adaptive differentiation frequency based advanced reference current generator in grid-tied PV applications. *IEEE J. Emerg. Sel. Top. Power Electron.* 1 (2019)
28. Babu, P.N., Peesapati, R.B., Panda, G.: A pre-filtering based current control strategy in grid-tied photovoltaic systems with active power filter for harmonic mitigation. In: *IEEE Region 10 Annual International Conference, Proceedings/TENCON*, pp. 1003–1008. IEEE (2019)
29. Smith, G.A., Onions, P.A., Infield, D.G.: Predicting islanding operation of grid connected PV inverters. *IEE Proc. Electr. Power Appl.* 147(1), 1–6 (2000)
30. Drude, L., Pereira Junior, L.C., Rüther, R.: Photovoltaics (PV) and electric vehicle-to-grid (V2G) strategies for peak demand reduction in urban regions in Brazil in a smart grid environment. *Renew. Energy.* 68, 443–451 (2014)
31. Erigrd. <http://erigrd.eu/transnational-access/selected-projects>. <http://erigrd.eu/trans.national.-access/selected-projects>
32. Papaioannou, I.T. et al.: Modelling and field measurements of photovoltaic units connected to LV grid. Study of penetration scenarios. *IEEE Trans. Power Deliv.* 26(2), 979–987 (2011)
33. Santhoshi, B.K. et al.: Critical review of PV grid-tied inverters. *Energies.* 12(10) (2019)
34. Zeb, K., et al.: A comprehensive review on inverter topologies and control strategies for grid connected photovoltaic system. *Renew. Sustain. Energy Rev.* 94, 1120–1141 (2018)
35. Coelho, V.N., et al.: Multi-objective energy storage power dispatching using plug-in vehicles in a smart-microgrid. *Renew. Energy.* 89, 730–742 (2016)
36. Esteves, R.M., Hacker, T., Rong, C.: Competitive K-means: a new accurate and distributed K-means algorithm for large datasets. *Proc. Int. Conf. Cloud Comput. Technol. Sci. CloudCom.* 1, 17–24 (2013)
37. Yang, L., Deng, M.: Based on k-means and fuzzy k-means algorithm classification of precipitation. *2010 Int. Symp. Comput. Intell. Des. ISC.* 2010. 1, 218–221 (2010)
38. Barzegkar-Ntovom, G.A. et al.: Generic dynamic load modelling using cluster analysis. *2018 53rd Int. Univ. Power Eng. Conf. UPEC.* 2018, 1–6 (2018)
39. Banerjee, S., Choudhary, A., Pal, S.: Empirical evaluation of K-means, Bisecting K-means, Fuzzy C-means and Genetic K-means clustering algorithms. In: *2015 IEEE Int. WIE Conf. Electr. Comput. Eng. WIECON-ECE 2015*, pp. 168–172 (2016)
40. Wang, X., Freitas, W.: Influence of voltage positive feedback anti-islanding scheme on inverter-based distributed generator stability. *IEEE Trans Power Deliv.* 24(2), 972–973 (2009)
41. Stevens, J., et al.: Development and testing of an approach to anti-islanding in utility-interconnected photovoltaic systems (2000)
42. IEEE standard for interconnecting distributed resources with electric power systems (2018)
43. ANSI/IEEE Std. 929-2000: IEEE recommended practice for utility interface of photovoltaic (PV) systems. (2000)
44. Teodorescu, R., Liserre, M., Rodriguez, P.: *Grid converters for photovoltaic and wind power systems*, 1st ed. John Wiley & Sons Inc (2011)
45. DIN VDE V 0126-1-1 (VDE V 0126-1-1): 2013-08: Automatic disconnection device between a generator and the public low-voltage grid. (2013)
46. IEC 62116:2014: Utility-interconnected photovoltaic inverters – test procedure of islanding prevention measures. (2014)
47. 'IEC 61000-3-3:2013: Electromagnetic compatibility (EMC) – Part 3-3: limits – limitation of voltage changes, voltage fluctuations and flicker in public low voltage supply systems, for equipment with rated current ≤16 A per phase and not subject to condition' (2013)
48. Alenius, H.: Modelling and electrical emulation of grid impedance for stability studies of grid-connected converters (2018)
49. Lu, M., et al.: Benchmarking of stability and robustness against grid impedance variation for LCL -Filtered Grid-Interfacing Inverters. *IEEE Trans. Power Electron.* 33(10), 9033–9046 (2018)
50. Suul, J.A. et al.: Impedance-compensated grid synchronisation for extending the stability range of weak grids with voltage source converters. *IET Gener. Transm. Distrib.* 10(6), 1315–1326 (2016)
51. Tedde, M., Smedley, K.: Anti-islanding for three-phase one-cycle control grid tied inverter. *IEEE Trans Power Electron.* 29(7), 3330–3345 (2014)
52. Cai, W. et al.: An islanding detection method based on dual-frequency harmonic current injection under grid impedance unbalanced condition. *IEEE Trans. Ind. Informatics.* 9(2), 1178–1187 (2013)
53. EN 50160: The main characteristics of the voltage at a network user's supply terminals in public low voltage, AC electricity networks under normal operating conditions, the limits or values of voltage characteristics. (2010)
54. The Experimental investigation on the performance characteristics of anti-islanding techniques in the prospect of high PV penetration level. (2018). <https://erigrd.eu/wp-content/uploads/2019/01/Technical-Report-Multyisland-Project-final>

55. Estébanez, E.J., et al.: 'Performance evaluation of active islanding-detection algorithms in Systems: two inverters case'. IEEE Trans. Ind. Electron. 58(4), 1185–1193 (2011)
56. Wu, L. et al.: Observation of inertial frequency response of main power grids worldwide using FNET/GridEye. IEEE Power Energy Soc. Gen. Meet. (2016)
57. Voglitsis, D., Papanikolaou, N., Kyritsis, A.C.: Incorporation of harmonic injection in an Interleaved Flyback inverter for the implementation of an active anti-islanding technique. IEEE Trans. Power Electron. 32(11), 8526–8543 (2017)
58. Voglitsis, D., Papanikolaou, N.P., Kyritsis, A.C.: Active cross-correlation anti-islanding scheme for PV module-integrated converters in the prospect of high penetration levels and weak grid conditions. IEEE Trans. Power Electron. 34(3), 2258–2274 (2019)
59. Voglitsis, D. et al.: On harmonic injection anti-islanding techniques under the operation of multiple der-inverters. IEEE Trans. Energy Convers. 34(1), 455–467 (2019)

How to cite this article: Boubaris A, Kyritsis A, Babouras K, et al. Study on the effectiveness of commercial anti-islanding algorithms in the prospect of mass penetration of PVs in low-voltage distribution networks. *IET Energy Syst. Integr.* 2021;3:39–59. <https://doi.org/10.1049/esi2.12007>